GEORGIA INSTITUTE OF TECHNOLOGY
OFFICE OF CONTRACT ADMINISTRATION
SPONSORED PROJECT INITIATION

Date: 5/23/79

Project Title: Evaluation of Low Cycle Fatigue Samples of Alloy 718

Project No: E-19-682 Green card

Project Director: Dr. T. H. Sanders, Jr.

Sponsor: General Electric, Gas Turbine Division

Agreement Period: From 5/2/79 Until 7/2/79

Type Agreement: Purchase Order No. A87-087-ZZZ-EXBM-0A1889 (under DOE Prime Contract EX-76-C-01-1806)

Amount: $4,052 (fixed price)

Reports Required: Final Letter Report

Sponsor Contact Person (s):

Technical Matters

Contractual Matters
(thru OCA)

Mr. W. P. Madigan
Gas Turbine Engineering and
Manufacturing Department
Building 53
P.O. Box 952
Schenectady, New York 12345

Defense Priority Rating: N/A

Assigned to: Chemical Engineering (School/Laboratory)

COPIES TO:

- Project Director
- Division Chief (EES)
- School/Laboratory Director
- Dean/Director–EES
- Accounting Office
- Procurement Office
- Security Coordinator (OCA)
- Reports Coordinator (OCA)
- Library, Technical Reports Section
- EES Information Office
- EES Reports & Procedures
- Project File (OCA)
- Project Code (GTRI)
- Other

CA–3 (3/76)

GEORGIA INSTITUTE OF TECHNOLOGY
OFFICE OF CONTRACT ADMINISTRATION

SPONSORED PROJECT TERMINATION

Date: April 17, 1980

Project Title: Evaluation of Low Cycle Fatigue Samples of Alloy 718

Project No: E-19-682

Project Director: Dr. T. H. Sanders, Jr.

Sponsor: General Electric, Gas Turbine Division

Effective Termination Date: July 2, 1979

Clearance of Accounting Charges: July 2, 1979

Grant/Contract Closeout Actions Remaining:

- x Final Invoice and Closing Documents
- _ Final Fiscal Report
- x Final Report of Inventions
- x Govt. Property Inventory & Related Certificate
- _ Classified Material Certificate
- _ Other _____

Assigned to: Chemical Engineering (School/Laboratory)

COPIES TO:

- Project Director
- Division Chief (EES)
- School/Laboratory Director
- Dean/Director–EES
- Accounting Office
- Procurement Office
- Security Coordinator (OCA)
- Reports Coordinator (OCA)
- Library, Technical Reports Section
- EES Information Office
- Project File (OCA)
- Project Code (GTRI)
- Other C. E. Smith

CA–4 (1/79)

FINAL REPORT

EVALUATION OF LOW CYCLE FATIGUE SAMPLES OF ALLOY 718

Submitted To:

Gas Turbine Division
General Electric Company
Schenectady, NY 12345

Submitted By:

T. H. Sanders, Jr.
Principal Investigator
Fracture and Fatigue Research Laboratory
Georgia Institute of Technology
Atlanta, Georgia 30332

ABSTRACT

A transmission electron microscopy (TEM) investigation was conducted on strain control fatigue (SCF) specimens of IN 718 received from the Gas Turbine Division of General Electric. The purpose of the investigation was to determine the nature of the cyclic deformation process as a function of strain range and temperature. Specimens cycled to failure at 204°C (400°F), 316°C (600°F), 427°C (800°F), 538°C (1000°F), and 649°C (1200°F) were characterized by TEM. At the three lowest temperatures, the principal mode of deformation was by mechanical twinning. However, at the two highest temperatures, the primary process for deformation was slip. The principal difference between the functional dependence of the strain-life behavior of the specimens cycled at 538°C and 649°C, and those cycled at the three lower temperatures (204, 316, 427°C) was interpreted in light of this change in deformation process with temperature. Limited scanning electron microscopy (SEM) revealed the presence of twins on the fracture surface and cracking along the twin-matrix interface was observed.

INTRODUCTION

Recent developments in the area of water cooled gas turbine design have necessitated a need for strain control fatigue (SCF) test data for IN-718 in the temperature range of 204°C (400°F) to 649°C (1200°F). To provide this information a number of SCF tests were conducted at Mar-Test. Inc., 45 Novner Drive, Cincinnati, Ohio 45215, under a program executed by the Gas Turbine Division of General Electric. These tests were carried out at 204°C (400°F), 316°C (600°F), 427°C (800°F), 538°C (1000°F), and 644°C (1200°F) to establish the cyclic plastic behavior of IN-718 in an elevated temperature environment. The results of this investigation are plotted in Figures 1 and 2 and can be summarized as follows:

1. The SCF data for IN-718 over the temperature and strain ranges investigated could not be adequately expressed according to the empirical "Coffin-Manson" relationship.[1,2] Mathematically, this relationship can be expressed in the form:

$$\Delta\varepsilon_p = \varepsilon_f' \, (N_f)^{-c}$$

where,

$\Delta\varepsilon_p$ - the cyclic plastic strain range,

ε_f' - the fatigue ductility coefficient,

N_f - the number of cycles to failure

c - the fatigue ductility exponent.

2. The strain-life plots could be classified according to two general responses.

   a. Those specimens which were tested at 204, 316 and 427°C were similar and could be represented by two linear relations in logarithmic coordinates, and

b. those specimens tested at 538 and 644°C had similar strain-life responses.

3. The results indicate that at low strains, Figure 1, lives were longer for specimens tested at the higher temperatures (538 and 649) compared to specimens tested at the lower temperatures (204, 316, and 427°C).

The purpose of this investigation was, therefore, to characterize the deformation behavior by transmission electron microscopy (TEM) of IN-718 as a function of plastic strain amplitude and test temperature, and with this microstructural information propose a mechanism to account for the observed behavior.

EXPERIMENTAL

The composition of the alloy is given in Table I. Table II summarizes the cyclic plastic strain amplitudes and the corresponding number of cycles to failure for the five test temperatures investigated.

TEM foils were prepared from selected LCF specimens and these are listed in Table III. Wafer approximately 0.5 mm thick were sectioned 2 mm below the fracture surfaces and discs 3 mm in diameter were punched from the wafer. The discs were electropolished by a twin jet polishing technique in a 2:1 - methanol: nitric acid solution cooled to -36°C. The foils were examined in a JEOL-JEM 100C electron microscope.

RESULTS

A series of micrographs are given in Figures 3-17 which illustrate the general deformation structures observed.

DISCUSSION

As reported by other authors[3] the TEM investigations confirmed the presence of microtwins which formed during the deformation process. Principally, twinning was confined to the lower temperatures 204°C (400°F), 316°C (600°F), and 427°C (800°F) and as reported by Fournier and Pinearu[3] the density of microtwins appeared to increase with increasing plastic strain range. At the two higher temperatures investigated the principal mode of deformation was slip.

CHARACTERIZATION OF THE DEFORMATION--TWINNING

The characterization of the planar deformation was based on two relevent observations. When the volume fraction of the planar defects was high, as in the case shown in Figures 3 and 4, diffuse intensity along matrix <111> directions was observed in the SAD patterns, Figures 5 and 6. The thickness of these planar defects, t, is significantly smaller than the length and width; consequently, the two dimensional characteristic of these defects caused strong two dimensional diffraction effects. Since the plane of the defects was parallel to {111} of the matrix, the streaks would be perpendicular to these planes, and thus lie along <111> directions, Figure 7.

The second point was the presence of extra reflections in the SAD patterns which would eliminate the possibility of stacking faults. Consequently, the defects were characterized as being fine twins which form during the deformation process.

Decreasing the strain-range appeared to increase the average spacing between the twin bands. For example, this can be seen by comparing Figures 3 and 4 with Figures 8 and 9.

Evidence of twinning can also be seen in Figures 10 and 11. These specimens were deformed at 427°C. Figure 11 also contains annealing twins shown at position A on the Figure.

CHARACTERIZATION OF THE DEFORMATION--SLIP

At the two higher temperatures (538°C and 649°C), the primary mode of deformation was thought to be by slip, (Figures 12 - 14) since streaking and extra reflections were not observed in the SAD patterns. Furthermore, when slip bands were observed, often incoherent particles were associated with these bands, suggesting that dislocations were generated at the interface between these particles and the matrix.

Occasionally, however, a favorably oriented grain may twin at the higher temperature. If after the twinning event occurs, successive deformation leads to slip, which is the predominate mode of deformation, the twin will become damaged, Figure 15. The observation of damaged twins has been made in other systems which undergo deformation by twinning and slip.[4] The damage of the twin does not occur uniformly since the growth of a deformation twin generates lattice defects which are not uniformly distributed in the vicinity of the twin interface.

INFLUENCE OF TWINNING ON THE FRACTOGRAPHY

A very limited SEM study showed that on specimens which were tested at temperatures which favored twinning, evidence of twin bands could be seen on the fracture surfaces, Figures 16 and 17. At high plastic strain ranges, very fine, intersecting twin bands could be seen, Figure 16, and on a specimen cycled at a similar temperature but at a comparatively lower strain range, the and spacing of the twin bands increased, Figure 17. These SEM observations complemented the TEM observations. Also, associated with the coarse twin bands were small secondary cracks as shown at position "A" in Figure 17.

TWINNING AS A MODE OF DEFORMATION

IN 718 can contain two types of strengthening precipitates, γ' and γ''. The volume fraction of the γ'' precipitate is larger for the heat treatment

given this material than γ'. Thus γ'' becomes the important precipitate in determining the basic deformation process. In an attempt to understand the behavior of IN 718, it is perhaps best to review some of the more important features of precipitation hardening alloys and how these ideas might be applied to understand the phenomena of twinning IN 718.

The strength of an alloy is related to the resistance to the motion of dislocations. Plastic deformation in FCC structures occurs by the motion of unit dislocations moving on close-packed planes, {111}, and in close packed directions, a/2 <110>.

The increase in flow stress of a precipitation hardening alloy is due to the interaction of dislocations with precipitates. Coherent and partially coherent precipitates may be penetrated by dislocations since the slip systems of the precipitates and the matrix are generally coincident. The strength and microdeformation characteristic of a precipitation hardening alloy will thus depend upon the degree of coherency, size, spacing, uniformity of the distribution of the precipitates and the crystallographic structure of the precipitate. For example, the microstructure and the influence of microstructure on the deformation behavior of γ/γ' alloys is fairly well understood. The crystal structure of the metastable γ' is the $L1_2$ structure and its relation to the FCC lattice is shown in Figure 18.

There are two unique types of lattice sites in this structure. The A sites are located on the faces of the cube. Since each face is shared by another unit cell, the six A sites contribute a total of three lattice points per unit cell volume. The B sites are located at the corners of the cube. Each site is shared by eight unit cells, and thus the total number of B lattice sites per unit cell volume is one. This arrangement leads to an A_3B structure. Initially, the four sites are equivalent; however, once a B site

is established the A sites are automatically defined since the structure must be consistent with the composition.

If deformation occurs and slip is activated in this structure, the motion of a unit dislocation in this ordered lattice will not recreate the structure in its wake, so disorder in the form of an antiphase boundary will occur, Figure 19. To eliminate the extra energy necessary to create the antiphase boundary, motion of an identical pair of unit dislocations is required, Figure 20. The separation of the two dislocations is determined by a balance between the force imposed by the structure to maintain its order and the repulsive force between the two dislocations of the same sign. It is the motion of two identical unit dislocations, super dislocations, which impart many of the properties to precipitation hardening nickel base alloys. Thus we are able to utilize information about the crystallography of the precipitate and develop a rational explanation about the deformation behavior of a γ/γ' alloy. Similarly we can use the same type of analysis to explain the observed twinning behavior in IN 718.

In IN 718, γ'' is the principal precipitate. γ'' is a DO_{22} phase which has the Ni_3Nb structure, Figure 21.[5] Figure 22 is a schematic of the DO_{22} structure. The stacking sequence of the DO_{22} is ABCDEFABCDEF. The motion of one pair of super lattice dislocations can restore the order as shown in Figure 22 but that is only true for one third of the slip systems. Along other slip systems the passage of four whole dislocations along the same plane is required to restore the order. Furthermore, the relationship between the matrix and the precipitate is:

$$(100)_{\gamma''} \parallel (100)_{\gamma}$$

$$[010]_{\gamma''} \parallel [010]_{\gamma}$$

thus there are three possible γ'' orientations in a given grain. Consequently, for any one slip system, one of these three sets of γ'' plates will have order

restored after shearing by two dislocations whereas the other two will require the passage of four dislocations to restore order.

As an alternative, Kirmen and Wellington proposed the dissociation of a unit dislocation into two partial dislocations, for example:

$$\frac{a}{2}[110] \rightarrow \frac{a}{6}[211] + \frac{a}{6}[12\bar{1}]$$

Schematically, this would lead to a stacking fault of the type ABAB in the precipitate. Kirmen and Wellington showed the presence of faulted precipitates.[5] The ABAB is the stable β phase.

The shearing mechanism by partial dislocations as given above can promote deformation by twinning. After shearing, one of the partial dislocations loops the precipitate. The loops eventually coalesce under the influence of internal stresses to propagate microtwins in the matrix. Consequently, we can develop a rational explanation which can account for the presence of the deformation twins in IN 718.

STRAIN CONTROL FATIGUE BEHAVIOR (SCF)

Investigators have used the analysis of Coffin and Manson to describe the SCF behavior of materials. Out of this research one fact continually emerges: numerous alloy systems do not strictly obey the relationship:

$$\Delta\varepsilon_p = \varepsilon_f' (N_f)^{-c}$$

there are three possible explanations which can be presented to account for the deviation. First, the nature of the deformation process may be affected by the plastic strain amplitude. For example, Saxena and Antolovich[6] studied the effect of stacking fault energy (SFE) on the fatigue deformation process in the Cu-Al alloy system. These authors observed that for high SFE alloys, the fatigue life plot was linear in logarithmic coordinates. However, for the low SFE alloys the fatigue life showed a distinct break. They attributed the

break to the inability of the dislocations to cross-slip at low plastic strain amplitudes when the SFE was low.

Alternatively, one can speculate that the presence of a break in the curve may be attributed to an environmental effect.[7] Coffin subscribes to the view that low cycle fatigue is principally a crack propagation process. Numerous investigators have shown the presence of microcracks as early as 10% of the life of the specimen; therefore, this view is realistic. At a specific frequency and elevated temperature, (Figure 23) large plastic strains produce a ductile mode of fracture which is a higher energy fracture process than granular fracture which occurs at low plastic strains. Thus at high temperatures, a break would be anticipated. One might carry this view one step further. At low plastic strain amplitudes, the life of the specimen is much greater than at a high plastic strain amplitude, thus the time at elevated temperature (or in a corrosive environment) is longer at a low plastic strain amplitude. At high strains, short times, the effect of either temperature or environment would be less than if the specimen were cycled at a comparatively low plastic strain amplitude. Consequently, the failure mechanism changes with the life of the specimen. At high PSA the failure is predominately mechanical where as at low PSA, the process is accelerated by the contribution of either temperature or environment.

The third possible explanation to account for the break in the curve depends upon the distribution of deformation.[8,9] The presence or absence of localized deformation is significant for two reasons: (1) these localized regions can act as initiation sites for fracture and (2) the magnitude of microplastic strain cannot be accurately measured by a conventional extensometer. Because the extensometer measures the average rather than the localized strain in the deformation bands, the Coffin-Manson plots for microstructures

which deform homogeneously at high plastic strains and heterogeneously at low plastic strains must exhibit non-linear behavior when the data are plotted on logarithmic coordinates.

Consequently, we have three distinct mechanisms to account for the temperature dependence of the strain-life behavior. Certainly we can not disregard the possibility that all three mechanisms could be operating simultaneously. Let us consider treating the data in accordance with the outlined mechanisms and perhaps arrive at a qualitative description of the phenomena.

In accordance with Saxena and Antolovich, changes in the deformation process alter the strain-life response. Since we have observed a difference in the deformation structure between the three lowest temperatures and the two highest temperatures we may postulate that the cyclic plastic behavior at 204, 316 and 427°C is dominated by deformation twinning and consequently the strain-life response for all those specimens are similar. However, at 538 and 649°C the predominate mode of deformation is slip and thus, the specimens tested at these temperatures will have a different strain-life response than those tested at the three lower temperatures.

Let us now consider the effect of temperature. According to Coffin, we would expect to see the break in the strain-life plot occur with an increase in temperature, Figures 23 and 24. However, analysis of the SCF data presented in Figure 1 shows that as temperature is increased to 538°C the break in the curve disappears. This result would tend to contradict that the presence of the break is purely a temperature effect. The effect of temperature, however, is most likely present when we compare the lives at similar strains at 538 and 649°C.

The concept of strain localization may account for the break in the curve when specimens were tested at the three lowest temperatures. The very localized nature of deformation twinning may account for this nonlinear behavior. As observed in this research and in the work of Fournier and Pineau[3] decreasing the strain amplitude increases the spacing between twin bands. The widely spaced, coarse twin bands may act as stress concentrators. Also, we did observe cracking along the twin-matrix interface in SEM. It is the view of this author that as we reduce the strain-amplitude we tend to localize the deformation and our macroview of the deformation structure gradually departs from the microview. If smaller gradations of $\Delta\varepsilon_p$ were used, we probably would observe a gradual departure from linearity.

In summary, we observed deformation twinning at 204, 316 and 427°C, and predominately slip at 538 and 649°C. The change in fatigue-life response between these two temperature groups has been attributed to this change in deformation.

REFERENCES

1. Coffin, L. F., Jr., Trans. ASME, 76, 931-950 (1954).

2. Manson, S. S., NACA Tech Note, No. 2933 (July 1953).

3. Fournier, D. and Pineau, A., Met. Trans. A, 8A, 1095-1105 (July 1977).

4. Chakrabortty, S. B., Mukhopadhyay, T. K., and Starke, E. A., Jr., Acta Met., 26, 909-920 (1978).

5. Kirman, I. and Warrington, D. H., Met. Trans., 1, 2667-2675 (October 1970).

6. Saxena, A. and Antolovich, S. D., Met. Trans., 6A, 1809 (1975).

7. Coffin, L. F., Jr., Journal of Materials, JMLSA, 6, No. 2 388-402 (June 1971).

8. Sanders, T. H., Jr., and Starke, E. A., Jr., Met. Trans., 7A, 1407 (1976).

9. Sanders, T. H., Jr., Mauney, D. A., and Staley, J. T., Fundamental Aspects of Structural Alloy Design, Ed. Robert I. Jaffee and Benjamin A. Wilcox, Plenum Publishing Corporation (1977).

10. Berling, J. T. and Slot, T., in Fatigue at High Temperatures, ASTM STP 459, American Society for Testing and Materials, p. 3 (1969).

TABLE I

COMPOSITION OF INCO 718

C	Mn	P	S	Si	Cr	Ni	Cu	Mo	Ti	Fe	Al	Co	B	(Cb+Ta)
0.05	0.01	0.005	0.004	0.12	18.28	51.93	0.03	2.88	1.03	20.06	0.47	0.12	0.005	5.01

TABLE II

TABULATED LOW CYCLE FATIGUE DATA OF IN 718

	Specimen Number	$\Delta\varepsilon_p$ (%) (measured at ½ life)	N_f (cycles to failure)
(400 F)	32	2.80	260
	31	0.98	2,217
	34	0.38	8,228
	39	0.09	40,717
	33	0.08	35,102
	36	0.04	86,234
(600 F)	11	2.88	321
	7	1.10	1,830
	12	0.38 'at $N_f/4$)	6,639
	30	0.04	70,968
(800 F)	10	2.84	314
	5	1.00	1,550
	9	0.36	5,922
	29	0.01	105,734 (run out)
(1000 F)	8	2.20	262
	19	1.08	959
	6	0.42	4,466
	37	0.09	167,284 (run out)
	4	0.13	50,025 (did not fail increased plastic strain to 0.96)
	4	0.96	756 (cycles at 0.96)
(1200 F)	2	0.86	452
	3	0.48	2,096
	1	0.18	15,533
	35	0.16	23,614

TABLE III

LOW CYCLE FATIGUE SPECIMENS SECTIONED FOR TRANSMISSION ELECTRON MICROSCOPY INVESTIGATION

Specimen No.	Test Temperature (°F)	$\Delta\varepsilon_p$ (measured) (%)
33	400	0.08
31	400	0.98
30	600	0.04
12	600	0.38 (at $N_f/4$)
29	800	0.01 (at termination)
9	800	0.36
37	1000	0.09
4	1000	0.96
35	1200	0.13
2 and 3	1200	0.86[2], 0.48[3]

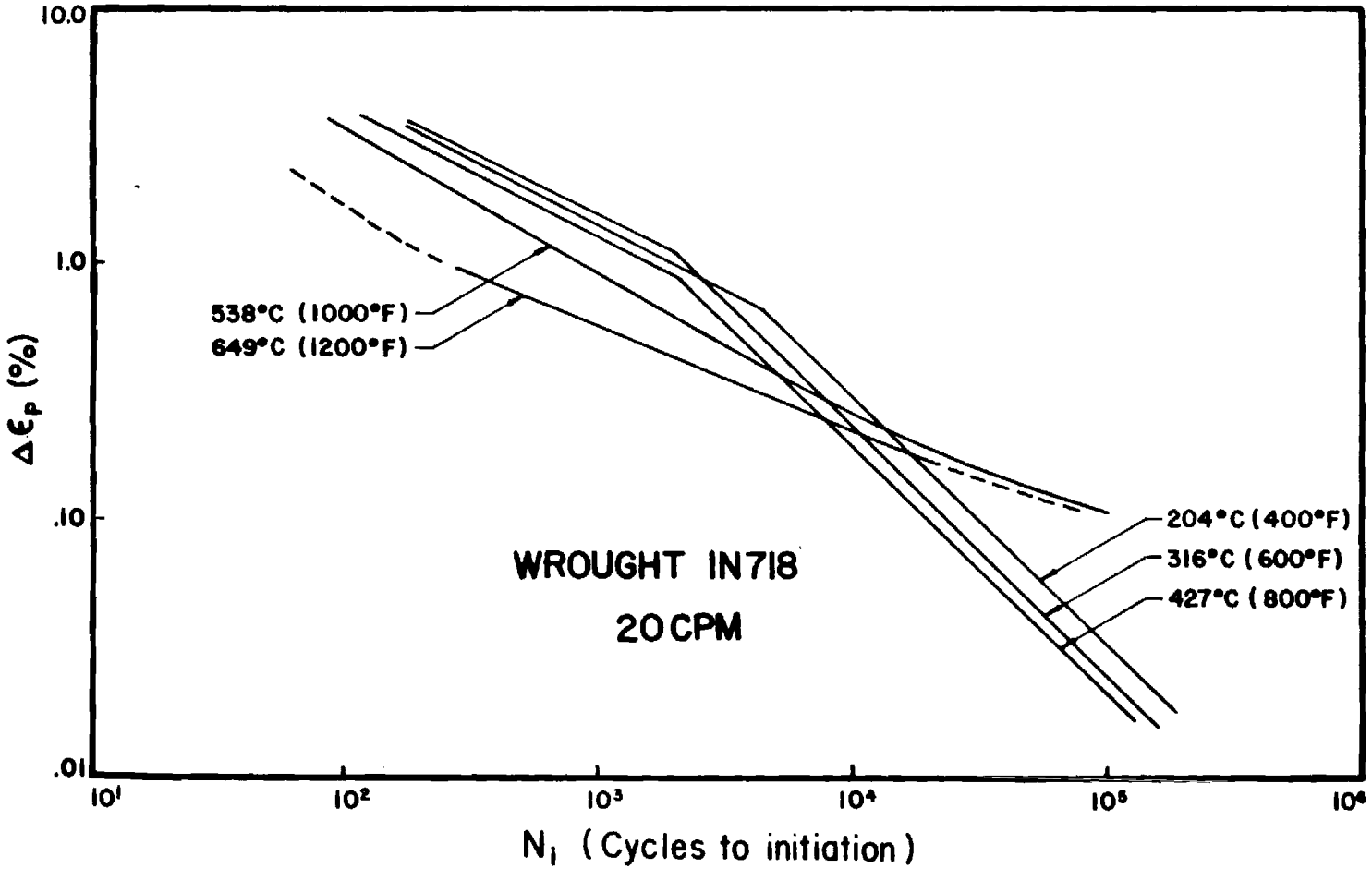

Figure 1. Plastic strain range versus number of cycles to initiation for IN 718 at variuos temperatures.

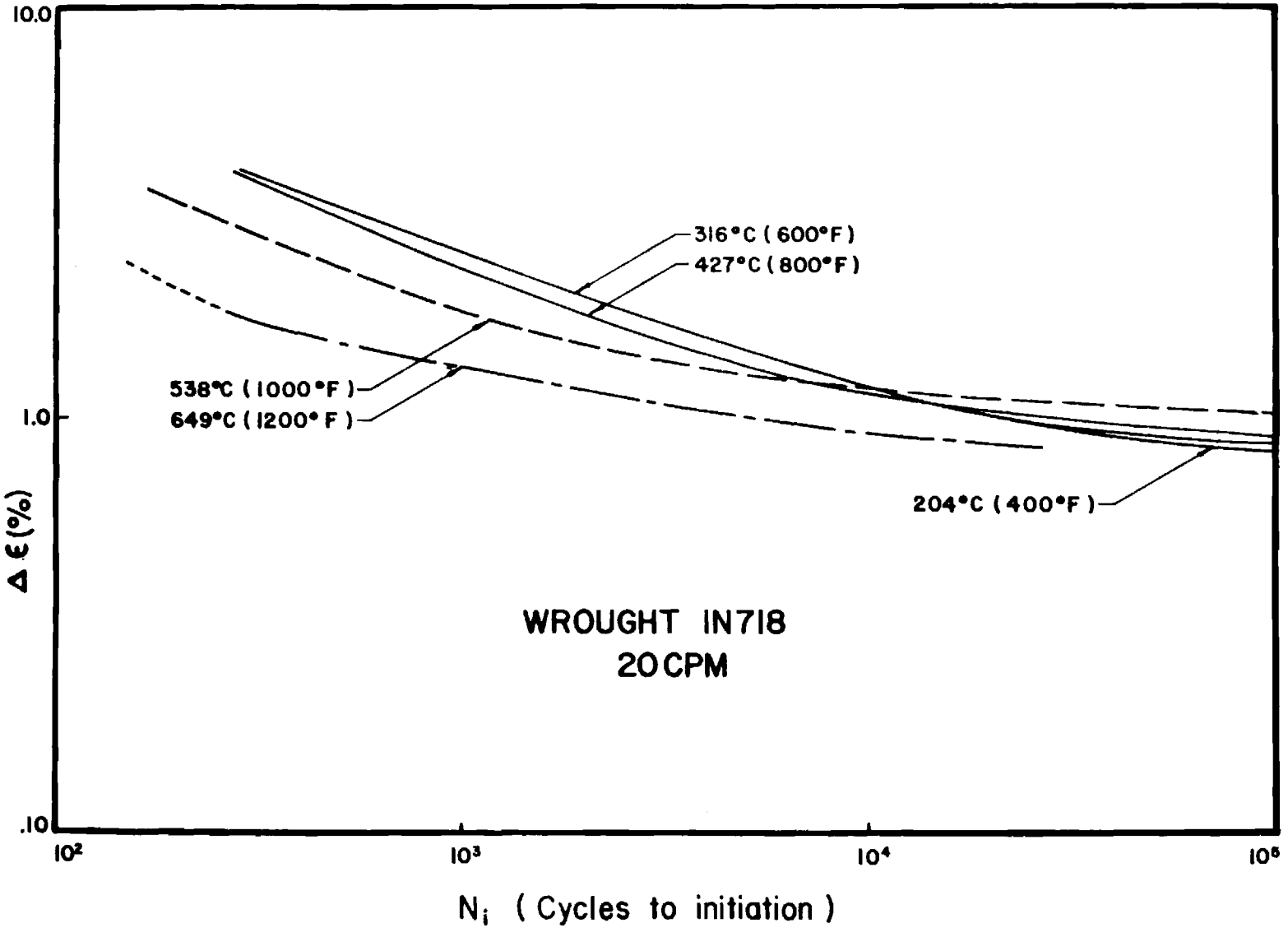

Figure 2. Total strain range versus number of cycles to initiation for IN 718 at various temperatures.

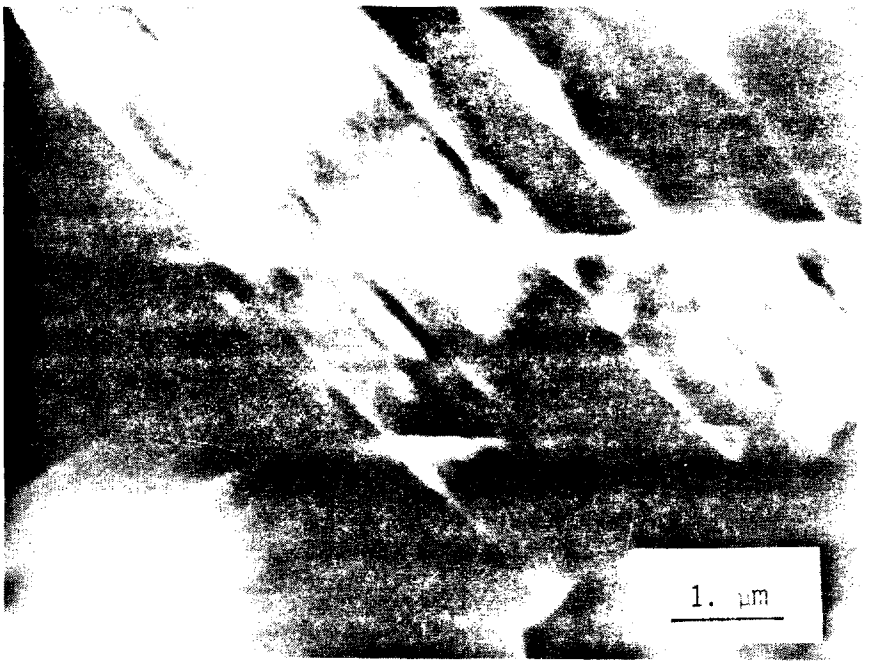

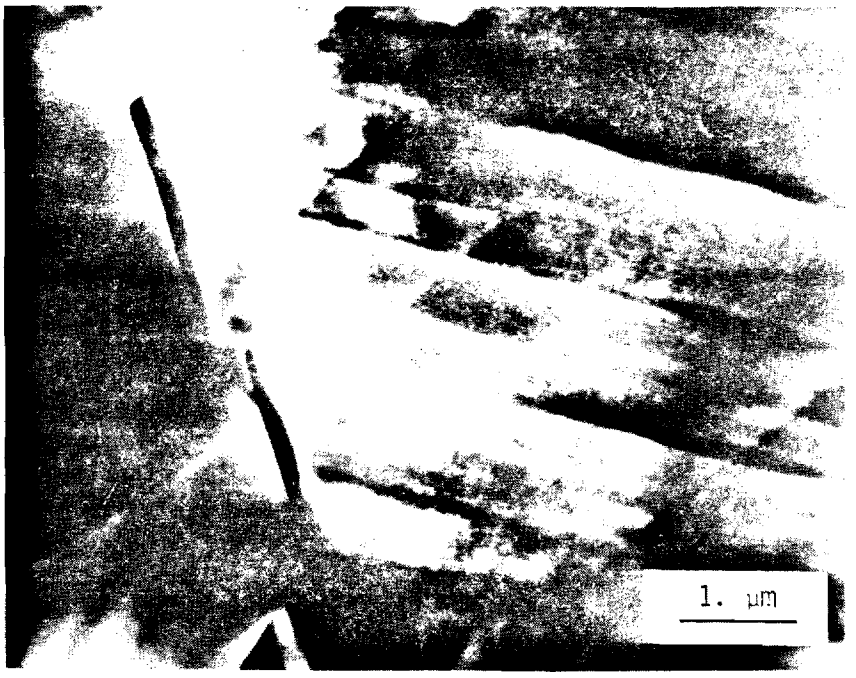

Figure 3. Electron micrographs showing the planar deformation features present in specimen 31.

Figure 4. TEM's showing the planar deformation features in specimen 31.

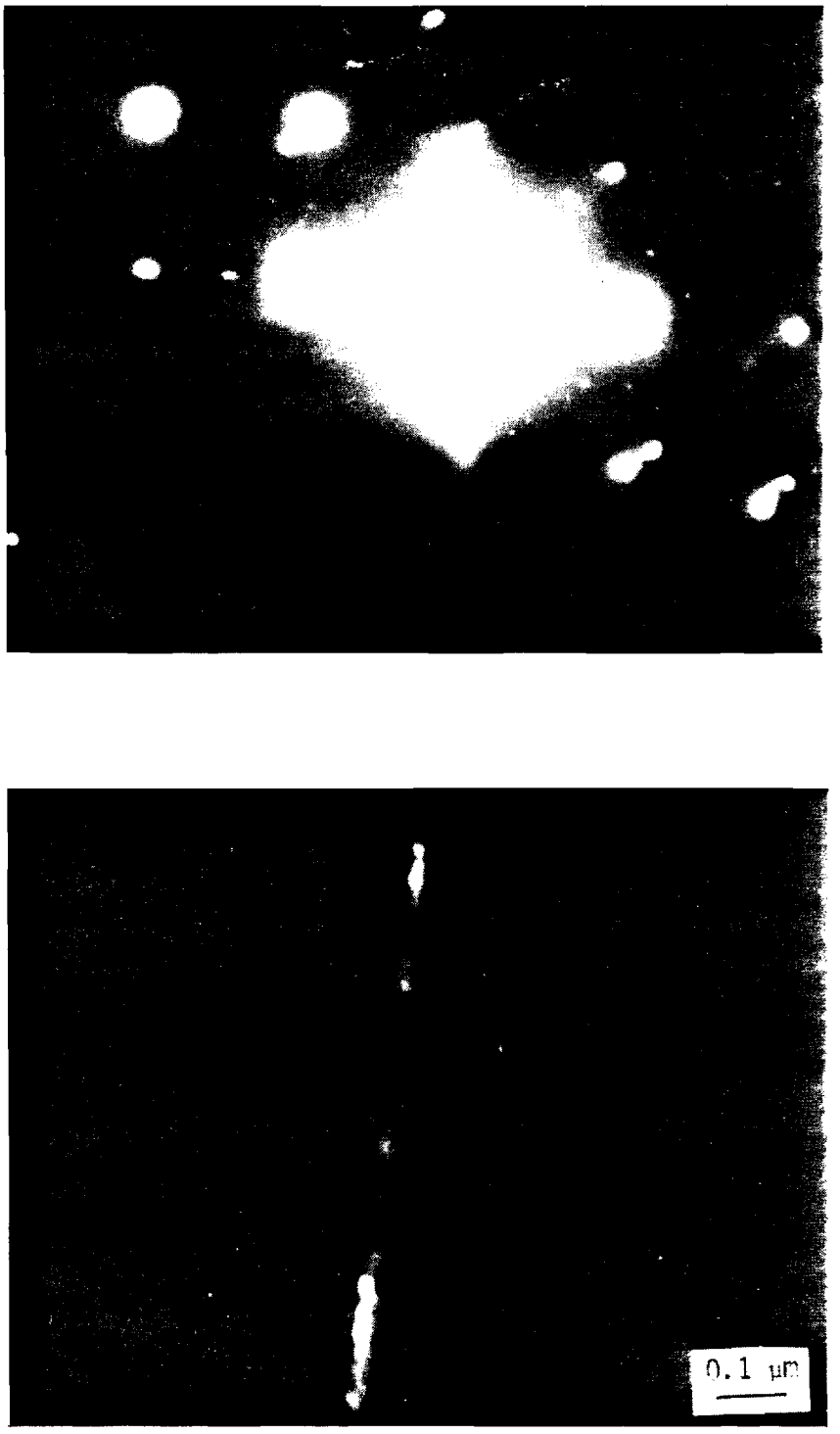

Figure 5. SAD and DF image showing that the extra reflections are associated with the planar defects (specimen 31).

Figure 6. B.F. of area in Figure 5.

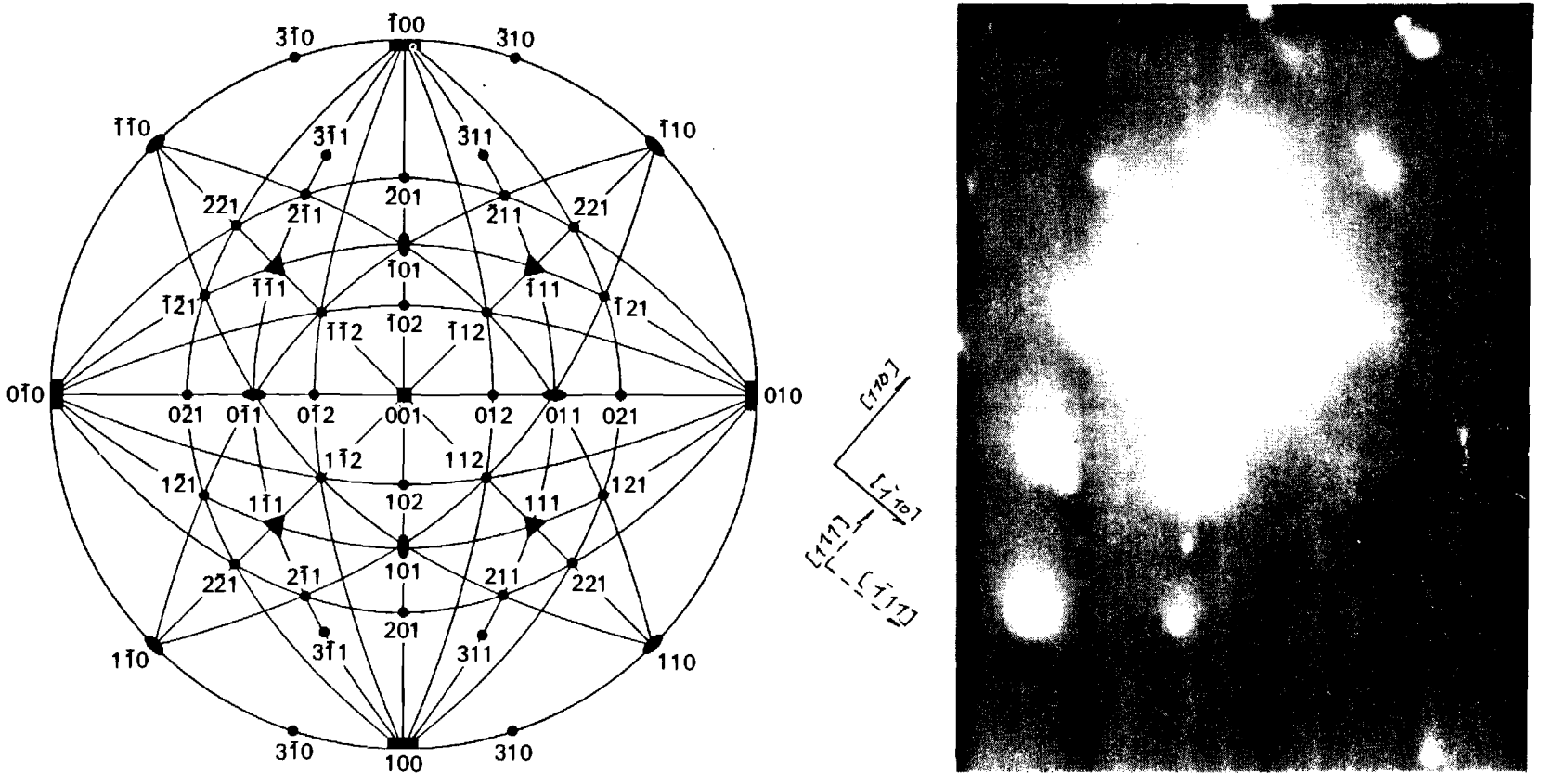

Figure 7. Stereographic projection and SAD illustrating the relationship between the diffuse streaks and the matrix <111> directions (specimen 31).

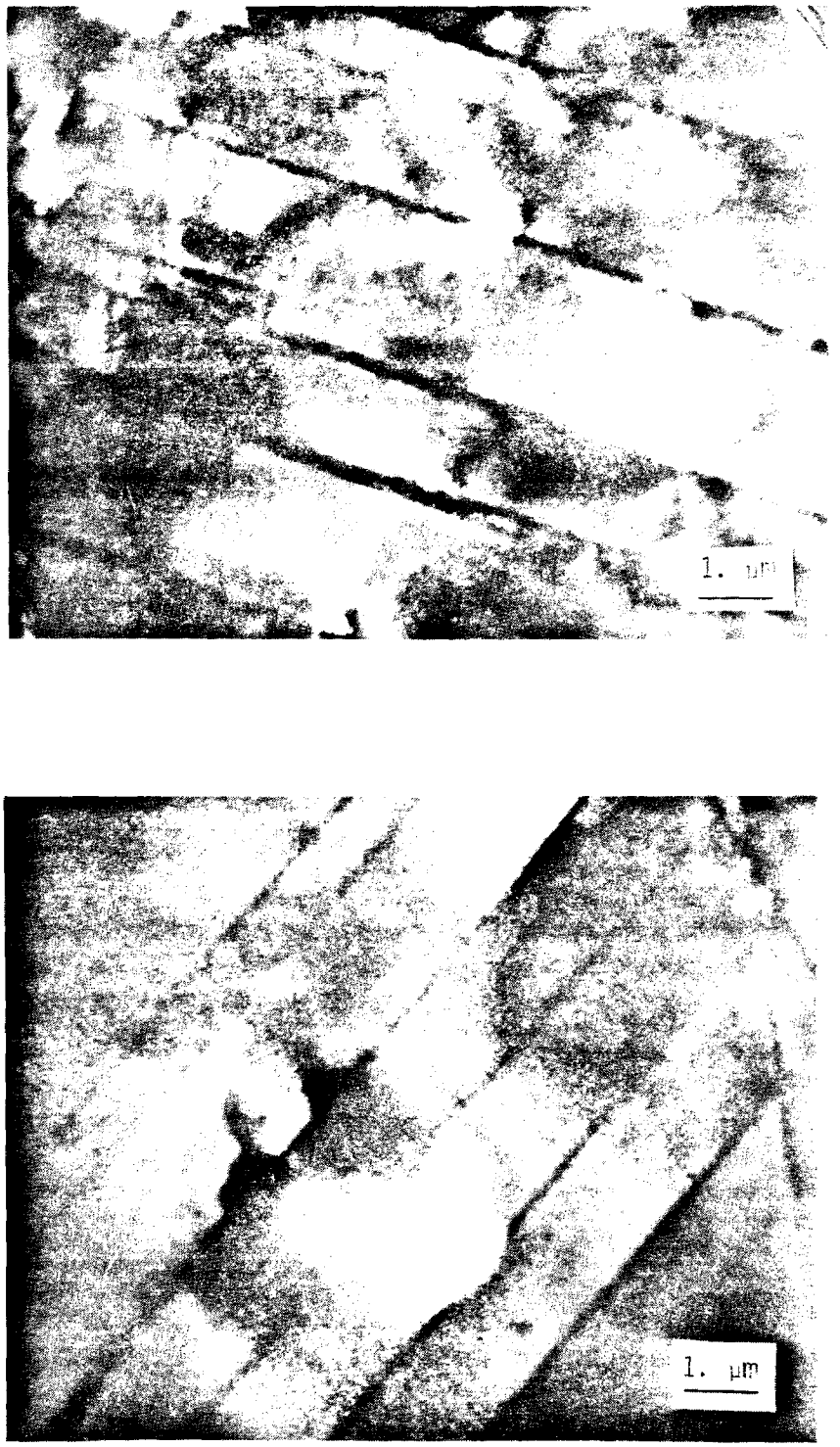

Figure 8. Deformation structure in specimen 34.

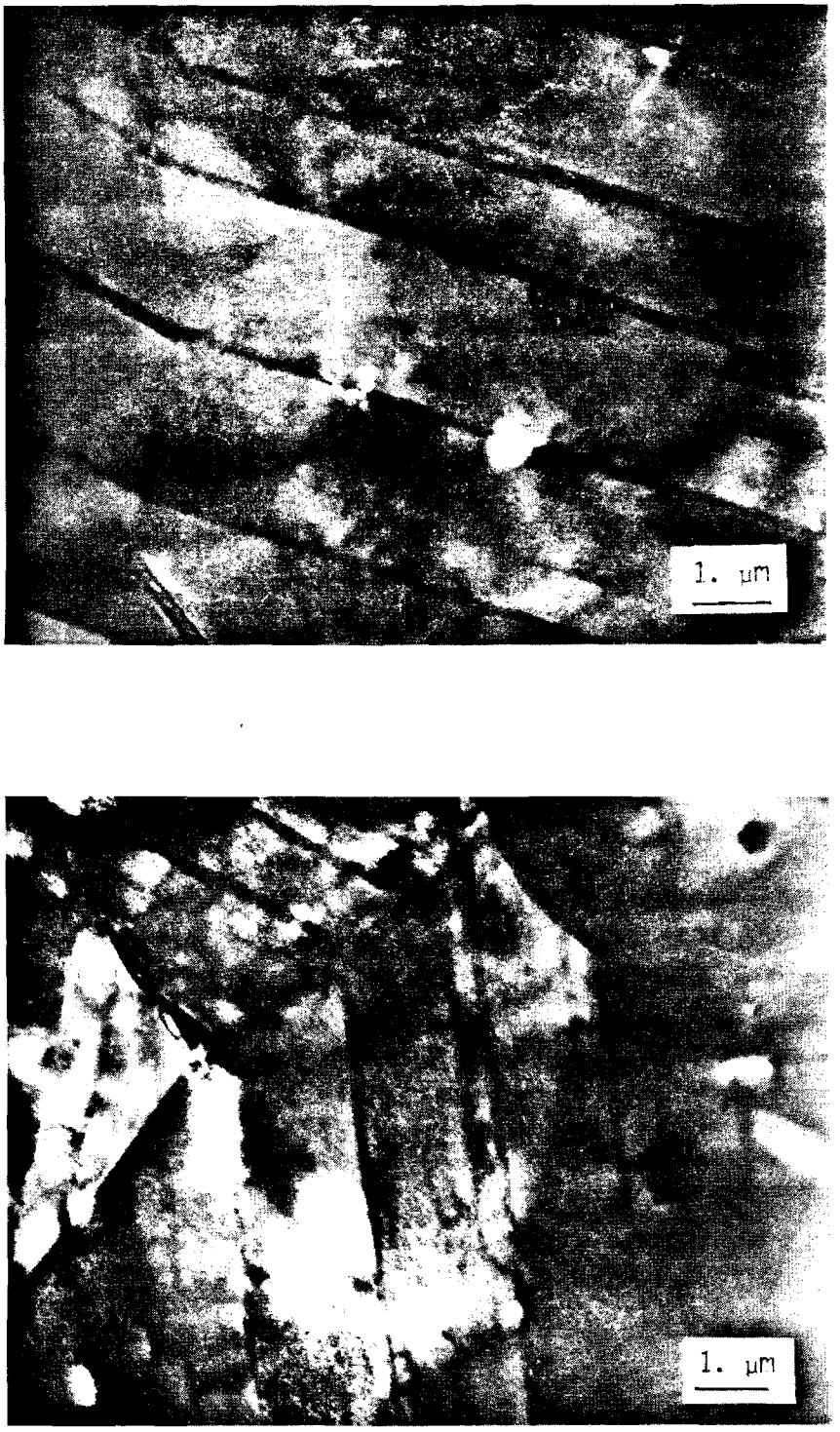

Figure 9. Deformation structure in specimen 34.

Figure 10. Deformation structure in specimen 9.

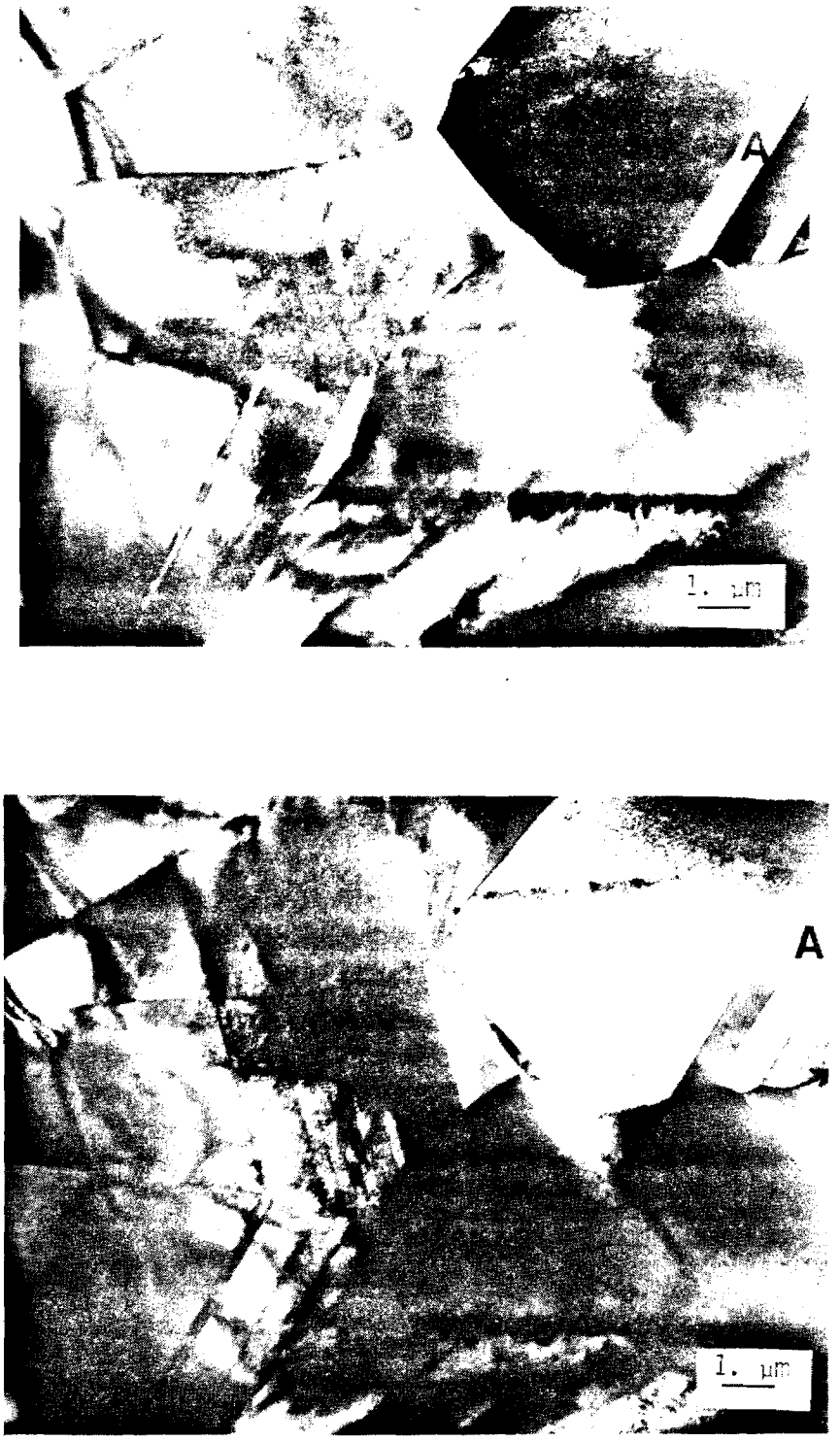

Figure 11. Deformation structure in specimen 9.

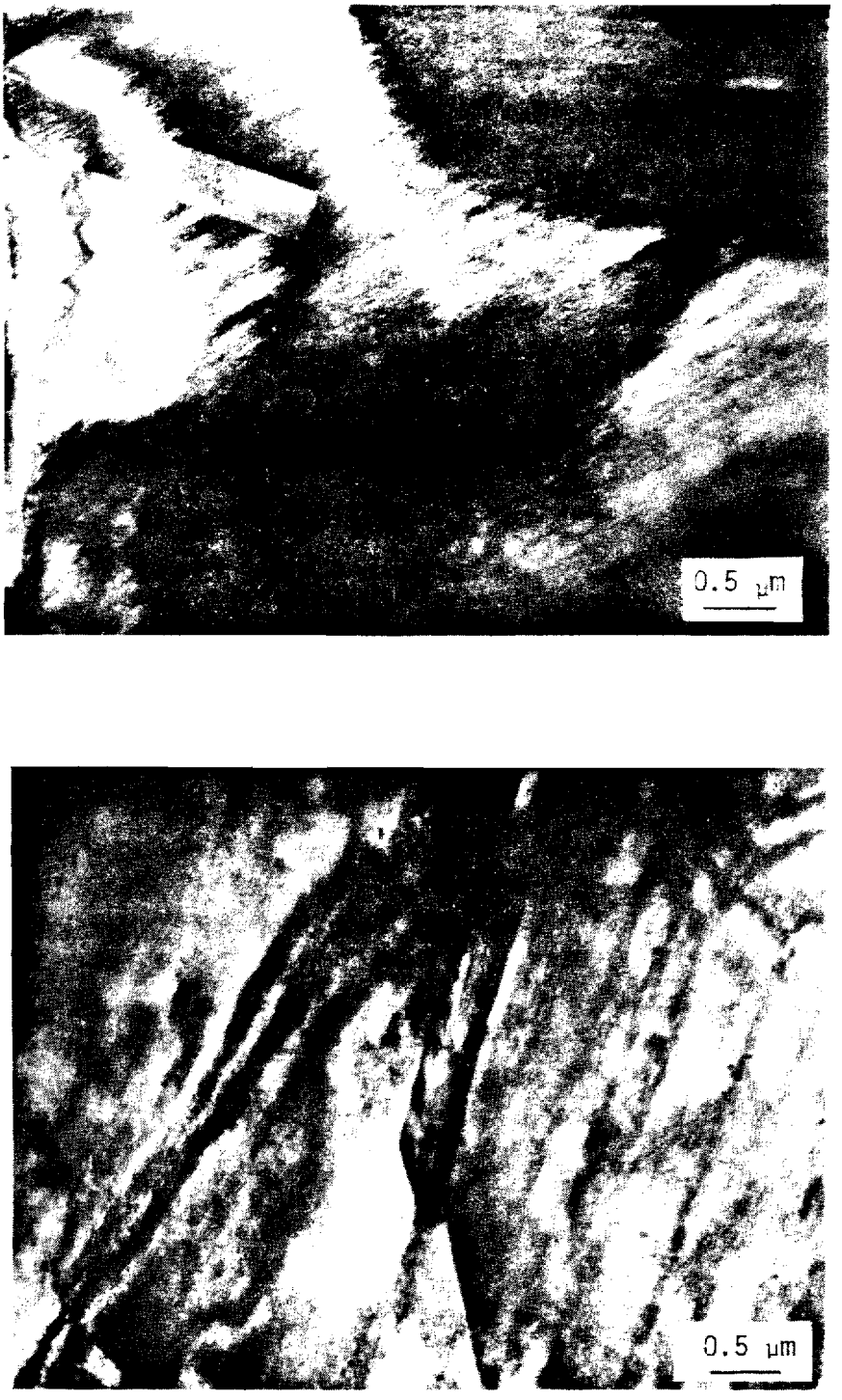

Figure 12. Deformation in specimen 4. Note the difference in the appearance of the deformation as compared to Figures 3 and 4, for example.

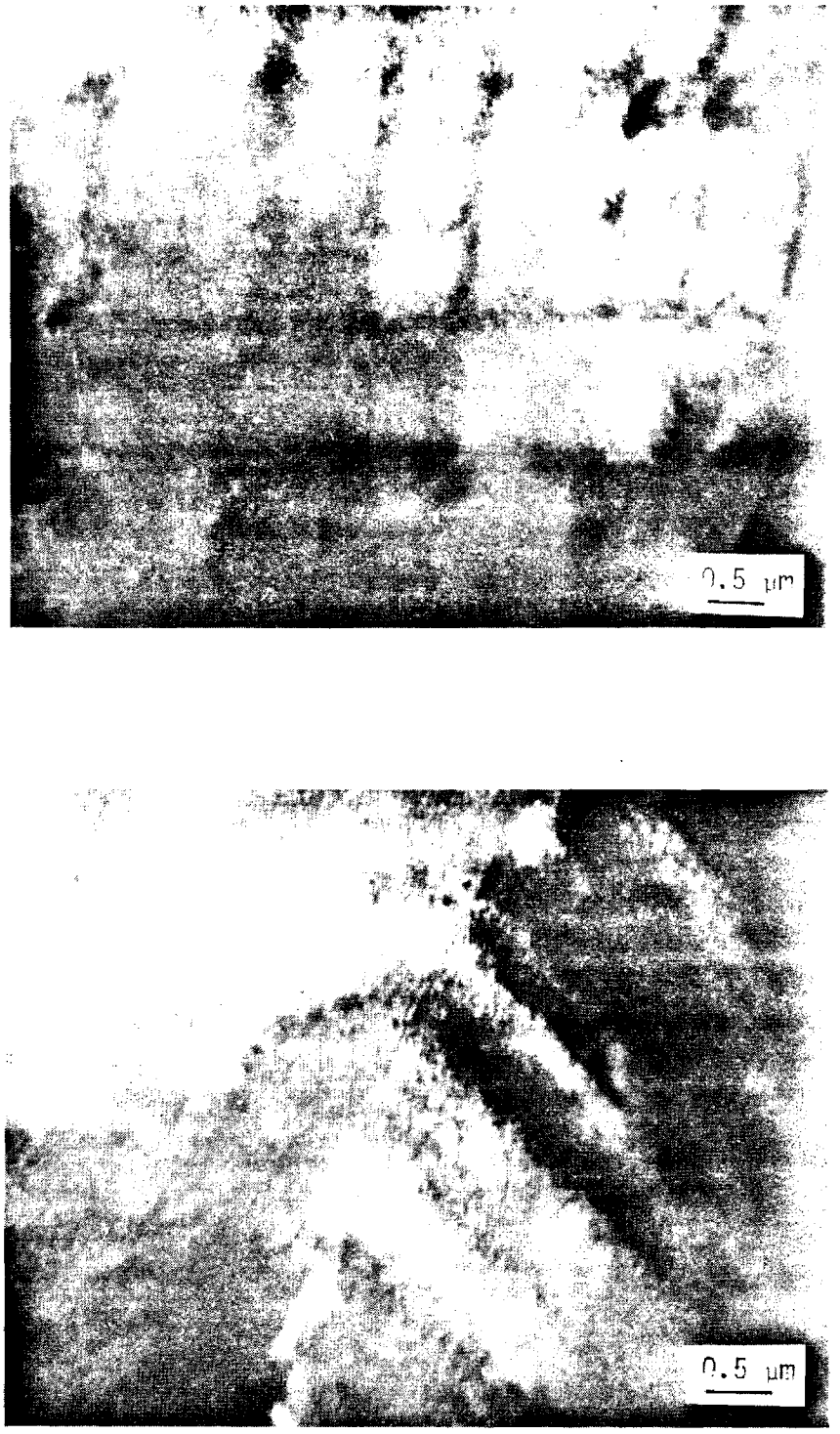

Figure 13. Deformation structure in specimen 4.

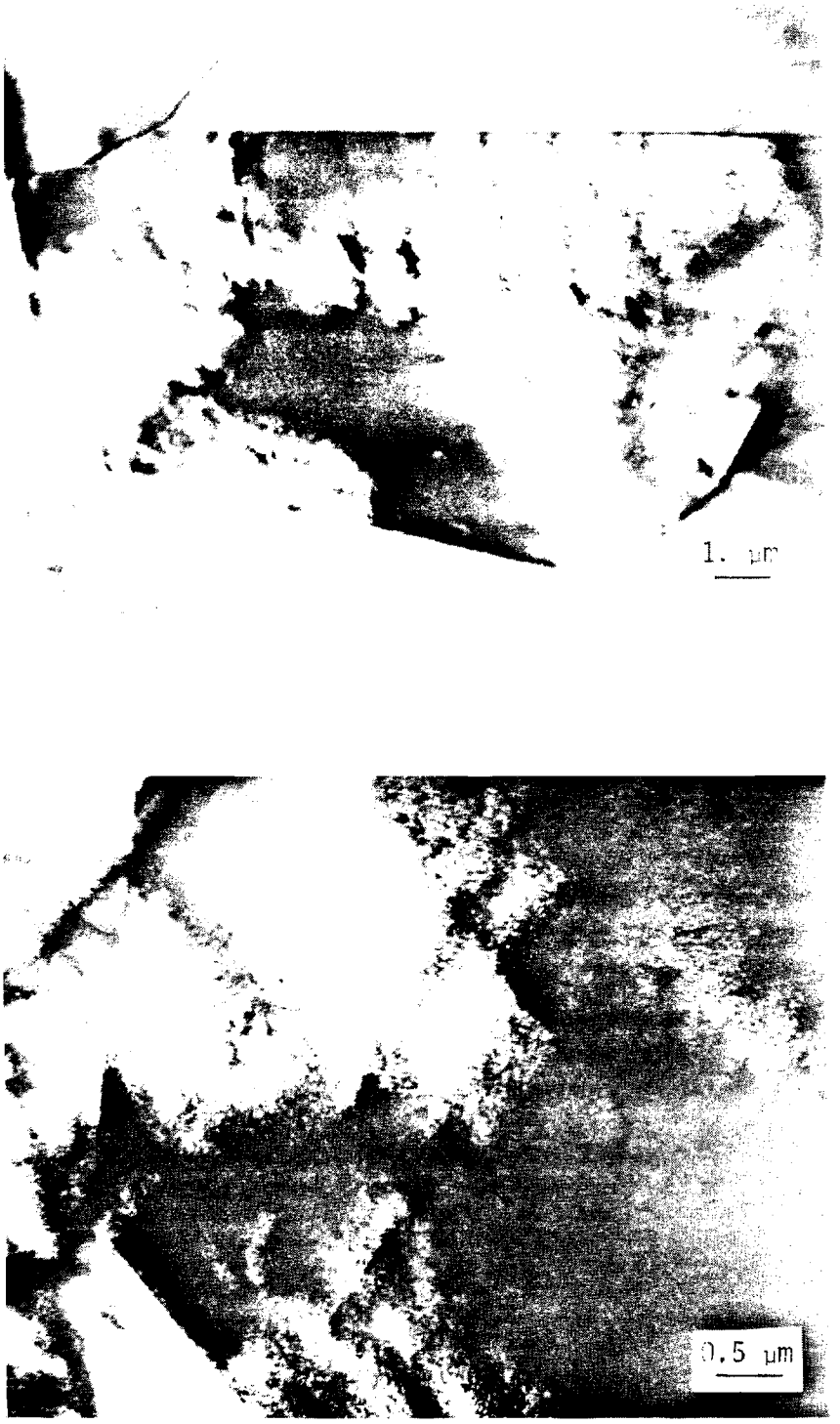

Figure 14. Deformation structure in specimen 3.

Figure 15. Deformation structure in specimen 35.

1100X

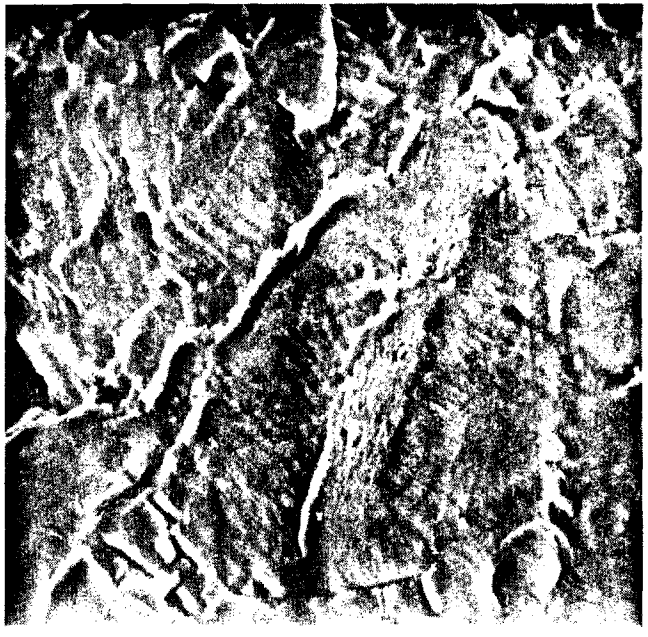

2200X

Figure 16. Fracture surface of specimen 31. Evidence of planar features on the fracture surface.

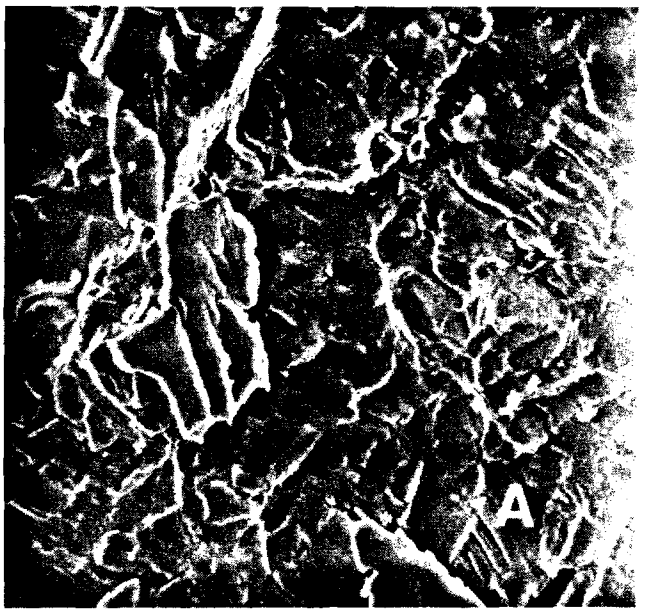

1100X

Figure 17. Fracture surface of specimen 30. Note the presence of small cracks at location A.

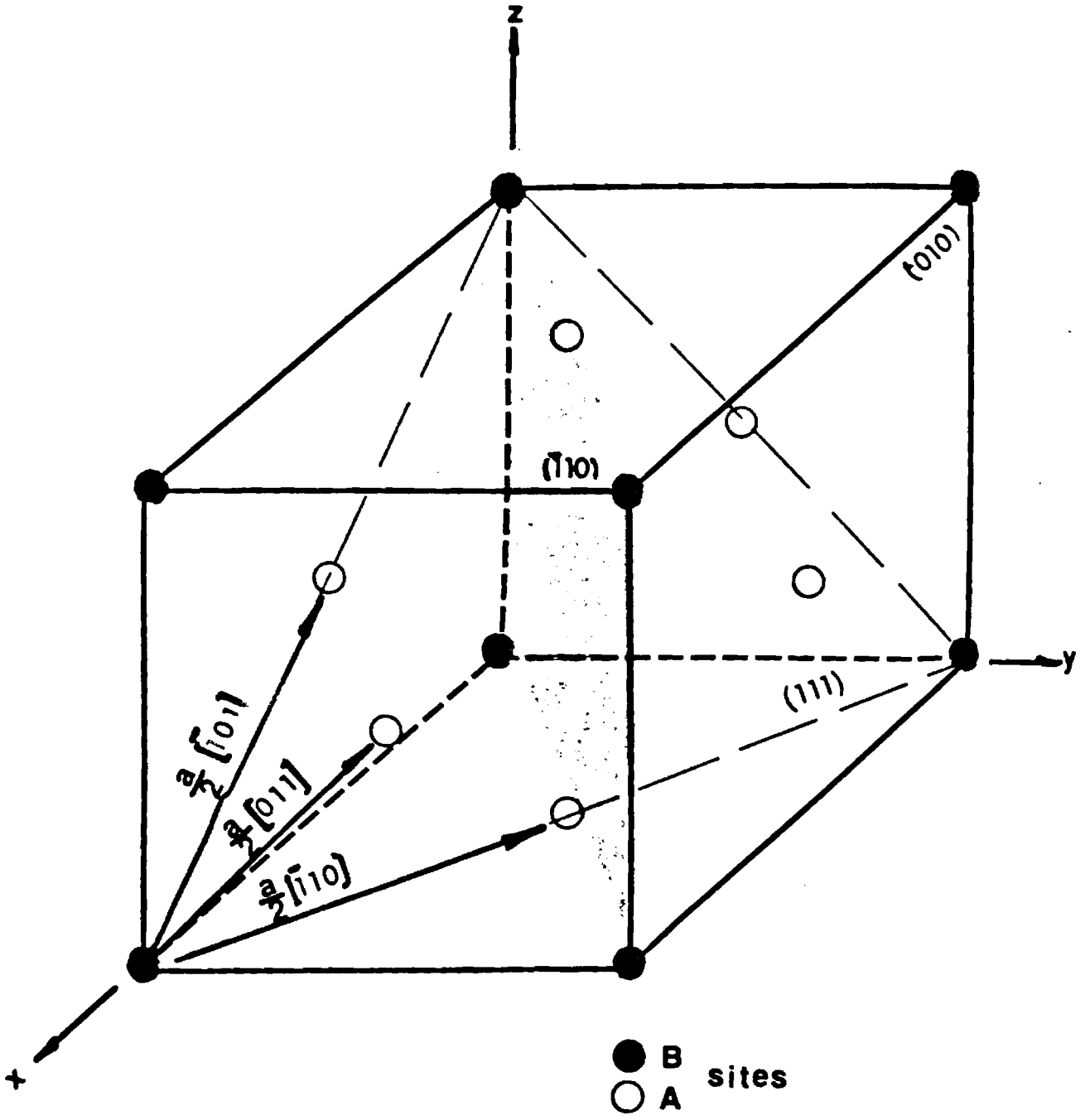

Figure 18. Definition of atomic positions in the face-centered, cubic (FCC) lattice.

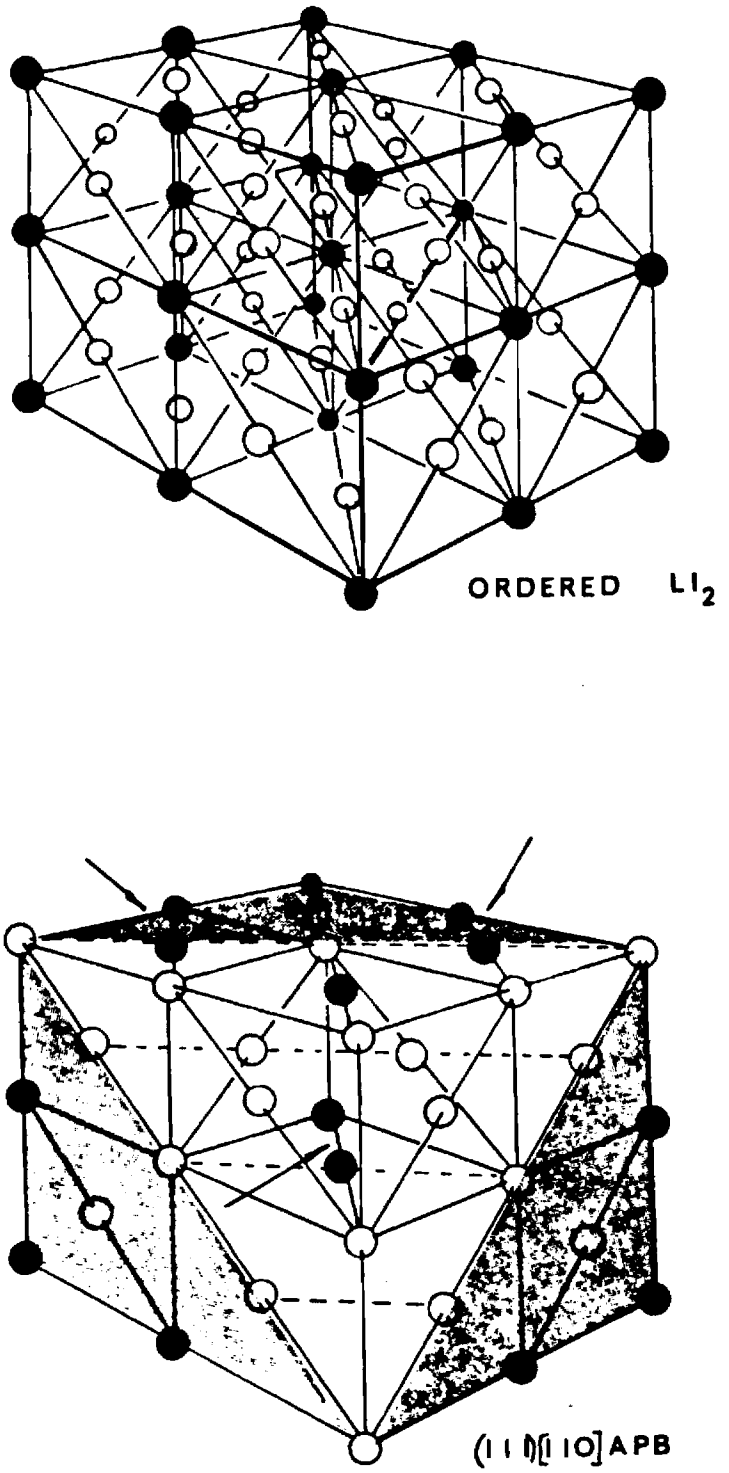

Figure 19. (a) The ordered Cu_3Au, $L1_2$ structure. (b) (111) [110] antiphase boundary in the $L1_2$ structure. Brackets show the creation of unlike neighbors.

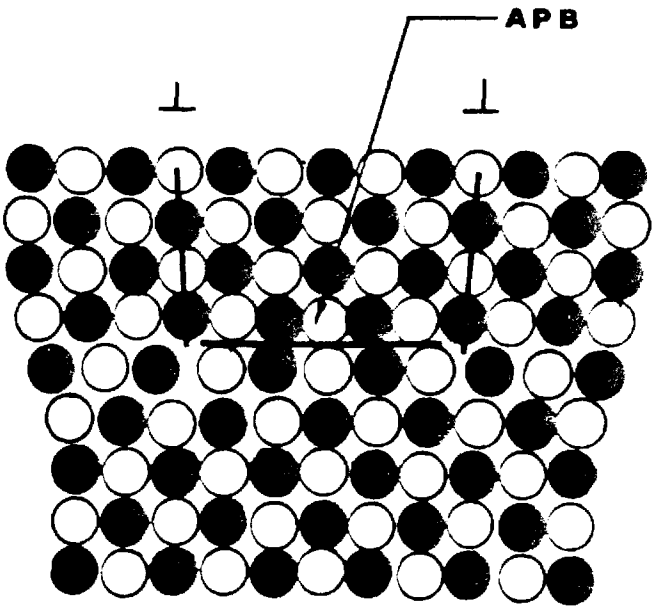

Figure 20. A (100) section through a region of ordered alloy illustrating the pair-wise motion of dislocations.

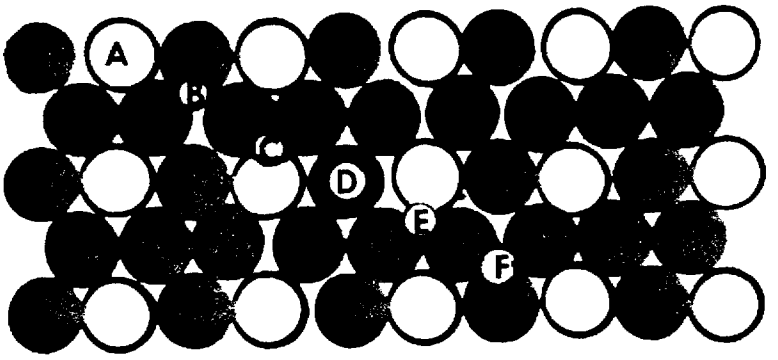

DO_{22} (Ni_3Nb)
SIX LAYER
STACKING
SEQUENCE
···ABCDEFABCDEF···

Figure 21. Stacking sequence in the DO_{22} structure.

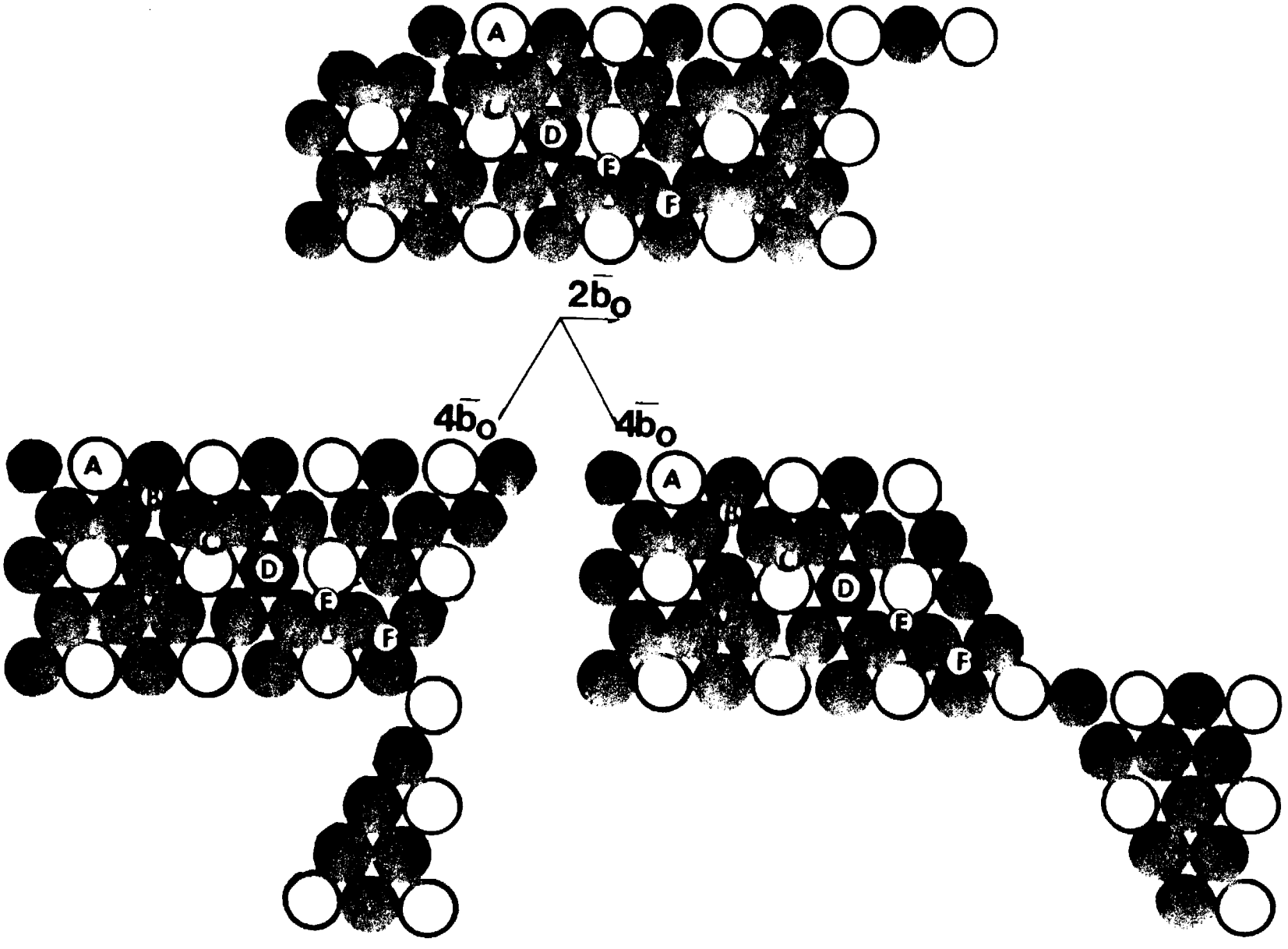

Figure 22. Schematic illustrating the requirements on the slip process to maintain the DO_{22} structure.

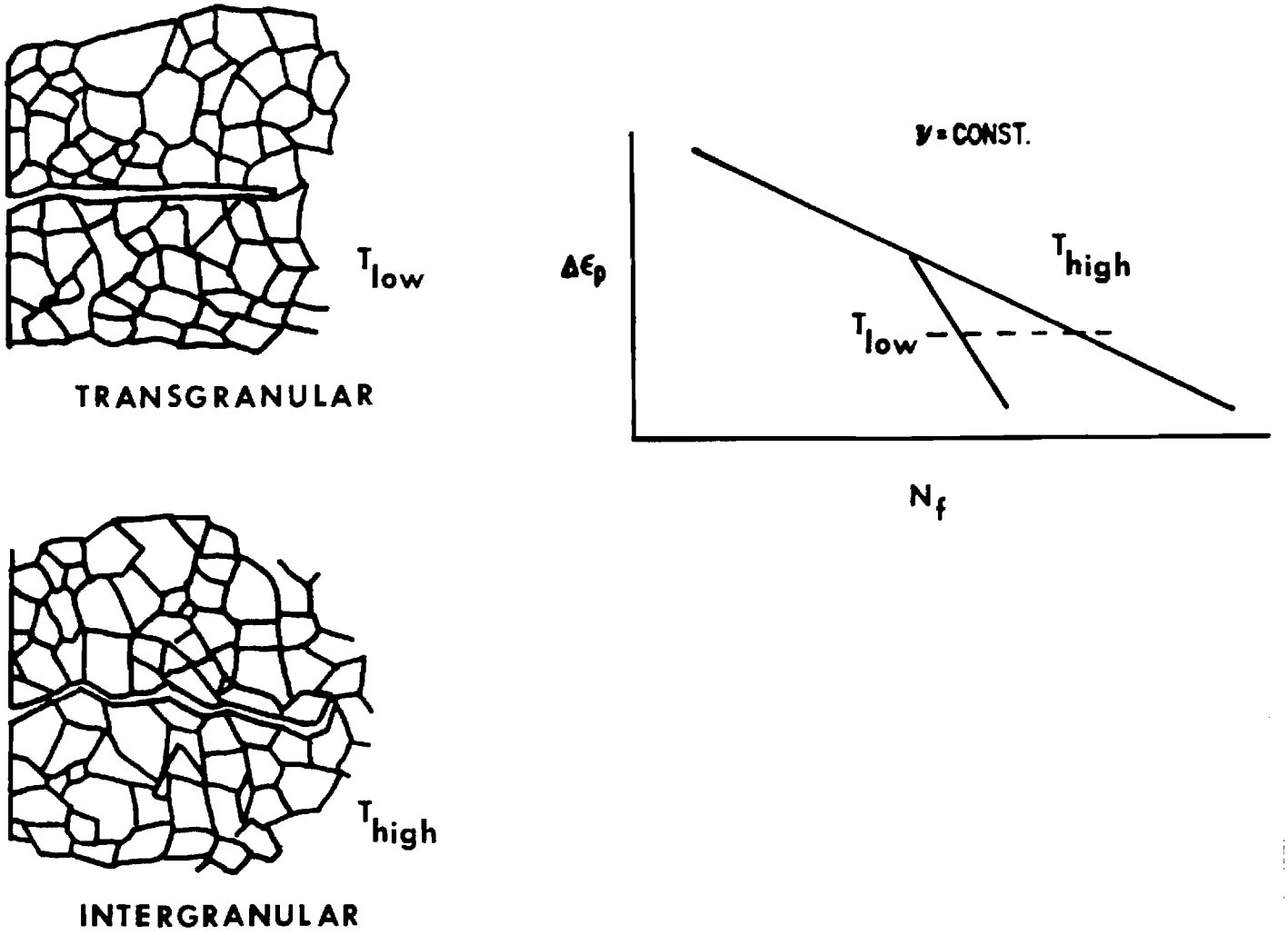

Figure 23. Schematic representation of fracture mode change with temperature and strain range (7).

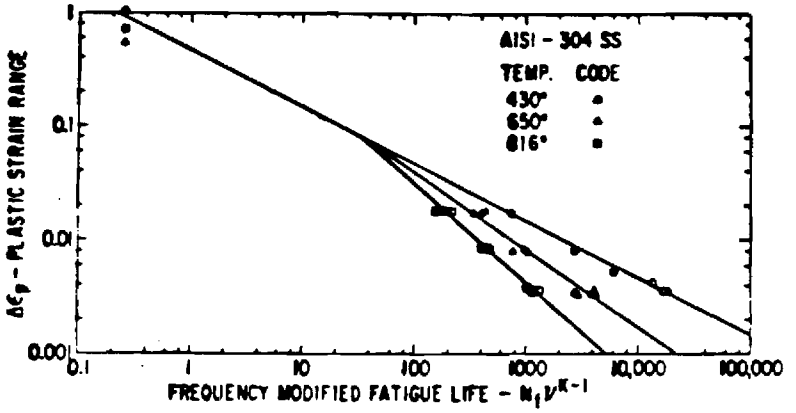

Figure 24. Plastic strain range versus frequency modified fatigue life of AISI 304 stainless steel (10).